https://doi.org/10.1016/j.energy.2018.10.161

Porous Co_3O_4 nanoplates as the active material for rechargeable Zn-air batteries with high energy efficiency and cycling stability

Peng Tan[1,2], Bin Chen[2], Haoran Xu[2], Weizi Cai[2], Wei He[2], Meng Ni[2,3,*]

1 Department of Thermal Science and Energy Engineering, University of Science and Technology of China, Hefei 230026, Anhui, China
2 Department of Building and Real Estate, The Hong Kong Polytechnic University, Hung Hom, Kowloon, Hong Kong, China
3 Environmental Energy Research Group, Research Institute for Sustainable Urban Development (RISUD), The Hong Kong Polytechnic University, Hung Hom, Kowloon, Hong Kong, China

[*]Corresponding Author, Tel: +852-27664152, E-mail: meng.ni@polyu.edu.hk (Meng Ni)

Abstract: Efficient electrocatalysts for oxygen reduction reaction (ORR) and oxygen evolution reaction (OER) are crucial for rechargeable Zn-air batteries. We report porous Co_3O_4 nanoplates with the average size and thickness of ~100 and ~20 nm, respectively, and a surface area of 98.65 $m^2\ g^{-1}$. The mesoporous nanostructure shortens the lengths for ion/electron transport and provides abundant reaction sites. In the alkaline solution, the Co_3O_4 nanoplates exhibit a comparable limiting current density to that of Pt/C in the ORR and a superior activity in the OER. Redox reactions corresponding to the oxidation/reduction of cobalt species with a high pseudocapacitance and stability are observed, indicating the multifunctional properties. Using Co_3O_4 nanoplates in the air electrode, the Zn-air battery delivers a maximum power density of 59.7 mW cm^{-2}. At a current density of 1 mA cm^{-2}, a gravimetric energy density of 901.6 Wh kg_{Zn}^{-1} and an energy efficiency of 67.3% are achieved. Moreover, the voltage gaps between discharge and charge as well as the energy efficiency of 58% at 10 mA cm^{-2} are maintained for 100 cycles. The porous Co_3O_4 nanoplate is a promising active material for efficient Zn-air batteries with excellent cycling stability and high energy density.

Keywords: Zn-air battery, cobalt oxide, porous nanoplate, multifunctional material, energy efficiency.

1. Introduction

To realize the long operation of electric vehicles and portable electronics, it is significant to develop advanced high-energy-density power systems [1,2]. Among various energy conversion and storage systems [3–6], rechargeable Zn-air batteries have become the research topic recently [7]. This is because metallic zinc is used as the reactant, which has a high theoretical capacity of 820 mAh g_{Zn}^{-1} [8]. Oxygen, as the other reactant, is taken from air instead of occupying the volume nor contributing to the weight of the battery. Thus, the theoretical energy densities can be superior to those of state-of-the-art lithium-ion batteries [9–12]. Particularly, different from Li-air and Na-air batteries that use highly active metals and aprotic electrolytes with numerous safety concerns [13], Zn-air batteries use aqueous alkaline electrolytes and are considered as highly safe and environmentally friendly [8]. Although the successful commercialization of primary Zn-air batteries has been achieved for a long time [2], the development of rechargeable ones is still on the initial stage. During discharge, gaseous oxygen molecules diffuse into the air electrode and are reduced at the triple-phase boundaries through the oxygen reduction reaction (ORR); while during charge, oxygen is released through the oxygen evolution reaction (OER) to the ambient air [14]. Hence, accelerating the ORR and OER is significant for the discharge and charge performance. However, the present Zn-air batteries suffer from the sluggish reaction kinetics, which results in the large discharge-charge voltages gap [15]. Consequently, the energy efficiency is greatly reduced. Besides, the large overpotentials can lead to the corrosion of the electrode material,

limiting the cycling stability [10]. Therefore, to improve the energy efficiency and ensure the long-term cycling stability, it is crucial to develop effective active materials of the air electrode [16,17].

Transition-metal oxides, due to their facile synthesis, remarkable activity, and low cost, have been reported as effective electrocatalysts in alkaline environments and applied in rechargeable Zn-air batteries [18–22]. Among them, cobalt oxides, especially Co_3O_4, have attracted great interests. In the spinel structure, the mixed valence of Co(II) and Co(III) enables the high ORR and OER activity [23]. To this end, Co_3O_4 has been used in the air electrode as a bifunctional electrocatalyst. For example, Zong *et al.* fabricated Co_3O_4 nanoparticle-decorated carbon nanofibers, which led to the higher energy efficiency of 64.0% and lower voltage gap of 0.9 V than those using Pt/C in the air electrode. [24]. Deng *et al.* synthesized an ultrathin Co_3O_4 nanofilm (1.8 nm) and achieved a lower overpotential of 0.72 V, a round-trip efficiency of 62.7%, and a long cycle life of 175 cycles at 2 mA cm^{-2} [25]. The good performance comes from the increased electrochemically active sites, large interfacial surfaces, and the enrichment of Co(III) ions on the surface. Wang *et al.* found that the surface crystal planes of Co_3O_4 are essential to promote the OER, and the crystal planes of {111} have the largest effect on reducing the overpotentials [26]. Chen *et al.* synthesized two-dimensional porous Co_3O_4 nanodisks with 500-600 nm in diameter and 20-40 nm in thickness [27]. Attributed to the special morphology though which both the mass diffusion and the charge transport were facilitated, a Zn-air battery showed stable charge and discharge voltages throughout 60 cycles with no voltage fading. Shirage *et al.* prepared two-dimensional hexagonal platelets of Co_3O_4 with (111) facets [28]. The highly crystalline Co_3O_4 plates have the

width of ~2 μm and the thickness of ~40-50 nm, and the specific surface area reaches 45.68 m^2 g^{-1}. In 2 M KOH, a high capacitance value of 305 F g^{-1} at 5 mV s^{-1} and a high capacity retention rate of 81.25 % after 2020 galvanostatic charge-discharge cycles were exhibited, indicating the potential application for electrochemical energy storage. Even with these promising results, the development of Co_3O_4 as the active material of the air electrode to achieve higher energy efficiency and cycling stability, especially at larger current densities, is still in urgent demand.

In this work, we report two-dimensional porous Co_3O_4 nanoplates as the active material for rechargeable Zn-air batteries. The (111) faceted hexagonal Co_3O_4 nanoplates with mesoporous nanostructure were fabricated through a facile method, which not only shortens the lengths for ion and electron transport but also provides abundant active sites. The electrochemical properties of the Co_3O_4 nanoplate were first examined in an alkaline solution. Then, a home-made Zn-air battery with Co_3O_4 nanoplates as the active material was built, and the discharge capacity and power density were measured. Further, the cycling performance was evaluated through a pulse discharge-charge test, and the stability as well as the energy efficiency were further analyzed.

2. Experimental

2.1 Synthesis of Co_3O_4 nanoplates

Co_3O_4 nanoplates were synthesized using a modified method as reported before [29,30]. Briefly, 0.16 mol KOH was first dissolved in 35 mL of distilled water, and then 5 mL of $Co(NO_3)_2 \cdot 6H_2O$ aqueous solution with the concentration of 4.0 M was slowly dropped into the KOH solution. After aging for 30 min with continuous stirring, the suspension was placed in an autoclave made of Teflon inside a stainless steel housing and

heated at 100 ^{o}C for 12 h. After cooling, distilled water and ethanol were used to wash the product thoroughly, followed by drying at 60 ^{o}C overnight. The dried powder was then heated using a furnace in air at 250 ^{o}C for 3 hours with 1 ^{o}C min^{-1} temperature ramp.

2.2 Physicochemical characterization

To observe the product morphology, a scanning electron microscope (SEM, VEGA3 TESCAN) and a transmission electron microscope (TEM, JEOL 2100F) were applied, which were operated under the voltage of 20 and 200 kV, respectively. The composition of the product was analyzed by a Rigaku Smartlab X-ray diffractometer (XRD) with a Cu-Kα source at 40 keV. To obtain the geometrical properties of the product, the nitrogen adsorption-desorption isotherm was measured by ASAP 2020, and the Brunaure-Emmert-Teller and Barrett-Joyner-Halenda methods were used to calculate the specific surface area and pore volume, respectively.

2.3 Three-electrode electrochemical analyses

A three-electrode cell with 0.1 M KOH as the electrolyte was used to evaluate the electrochemical properties, which were measured using a Solartron potentiostat by rotating disc electrode (RDE) voltammetry. The ink solution was prepared by physically mixing 4 mg of prepared Co_3O_4 nanoplates, 2 mg of active carbon (Vulcan XC-72), and 20 μL of Nafion solution (5 wt%) into 380 μL of isopropanol, followed by ultrasonicating for 30 minutes to make it homogeneously. Then, 4 μL of the ink was carefully dripped onto the polished glassy carbon electrode (diameter: 4 mm) and dried completely to form the working electrode with the catalyst loading of 0.2 mg cm^{-2}. To make a comparison, the Pt/C electrode was made with the similar approach by replacing the Co_3O_4 nanoplates

with the commercial 20% Pt/C catalyst. The counter electrode was a platinum wire, and a Hg/HgO electrode was used as the reference electrode.

To characterize the ORR activity, oxygen gas was first purged to saturate the electrolyte. Linear sweep voltammetry (LSV) for ORR polarization curves was conducted within the potential range from 0.2 to −0.7 V (vs. Hg/HgO) using the rotation speeds from 400 to 2500 rpm, and a scan rate of 5 mV s^{-1} was applied. The kinetic current (j_k,) was obtained using the Koutecky-Levich equation [31]:

$$j^{-1} = j_k^{-1} + j_d^{-1} \tag{1}$$

$$j_d = 0.2nFD_{O_2}^{2/3}\nu^{-1/6}C_{O_2}\omega^{1/2} \tag{2}$$

where j is the measured current density and j_d is the diffusion-limiting current densities. n is the number of electrons transferred, F is the Faraday constant (96485 C mol^{-1}), and ω is the angular velocity (rpm). D_{O_2} and C_{O_2} are the diffusion coefficient and the bulk concentration of O_2 in 0.1 M KOH, the values of which are 1.86×10^{-5} cm^2 s^{-1} and 1.21×10^{-6} mol cm^{-3}, respectively. ν is the kinematic viscosity of 0.1 M KOH, and the value is 1.01×10^{-2} cm^{-2} s^{-1}. To measure the OER activity, the LSV curve was conducted within the potential range from 0.2 to 0.9 V (vs. Hg/HgO) using a rotation speed of 1600 rpm at 5 mV s^{-1}. The Cyclic voltammetry (CV) results were obtained using RDE at various scan rates within 0.3−0.8 V (vs. Hg/HgO), and the stability test was conducted at 50 mV s^{-1}. The measured current densities were normalized by the area of glassy carbon, and the specific capacitance was calculated based on the following equation [32]:

$$C = \frac{1}{ms(V_f - V_i)}\int_{V_i}^{V_f} I\mathrm{d}V \tag{3}$$

where m is the mass loading of Co_3O_4 nanoplates, s is the scan rate, V_f and V_i present the potential range of the voltammetric curve (0.2−0.9 V), and I is the current density. To clearly present the results, a reversible hydrogen electrode (RHE) was used for the calibration [33]:

$$E_{RHE} = E_{Hg/HgO} + 0.059\text{pH} + 0.098 \quad (4)$$

2.4 Battery fabrication and evaluation

The working electrodes were prepared by spraying the ink onto a carbon paper (Toray TGP-H-060), which was a mixture of 50% of active carbon (carbon power of Vulcan XC 72 (20-40 nm) and carbon nanotubes (40-60 nm in diameter and 5-15 μm in length) with the weight ratio of 1:1) [34], 25% of active material (Co_3O_4 nanoplate or Pt/C), and 25% of polytetrafluoroethylene (PTFE) binder. The loading of the catalyst on the air electrode was 2 mg cm^{-2}. A Zn-air battery was composed of a Zn foil as the metal electrode, the as-prepared air electrode, and 6 M KOH + 0.2 M zinc acetate as the electrolyte, as the photograph shown in **Fig. S1** (Supporting information) [35]. The galvanodynamic charge and discharge voltage profiles of the battery were measured at a current step of 1 mA s^{-1}. The galvanostatic discharge voltage curves were measured at the current density of 1 mA cm^{-2}, and the discharge capacities (mAh g^{-1}) were calculated based on the consumed zinc. The cycling stability was tested at 10 mA cm^{-2} with a fixed time interval (360 s for discharge followed by 360 s for charge).

3. Results and discussion

3.1 Material characterization

The SEM image is presented in **Figs. 1a** and **S2**, from which the synthesized nanoplates with the lateral size of 111.7 ± 16.9 nm and the thickness of ~20 nm are

observed, which are in much smaller dimensions than those of previously reported [26–28]. The TEM images in **Figs. 2b** and **2c** clearly demonstrate the hexagonal shape of the nanoplates with a porous structure, which is attributed to the release of water molecules during the calcination process [36]. From **Fig. 2c**, the nanoplate is composed of nanoparticles with sizes of ~8 nm and pores of ~3 nm. A high-resolution TEM image of this individual nanoplate in **Fig. 2d** corroborates the interplaner spacing of 0.244 nm, which corresponds to the (311) plane of Co_3O_4, and the selected-area electron diffraction (SAED) pattern corroborates the (220), (311), (400), (511), and (440) planes of crystalline Co_3O_4. These results confirm that porous Co_3O_4 nanoplates were successfully synthesized.

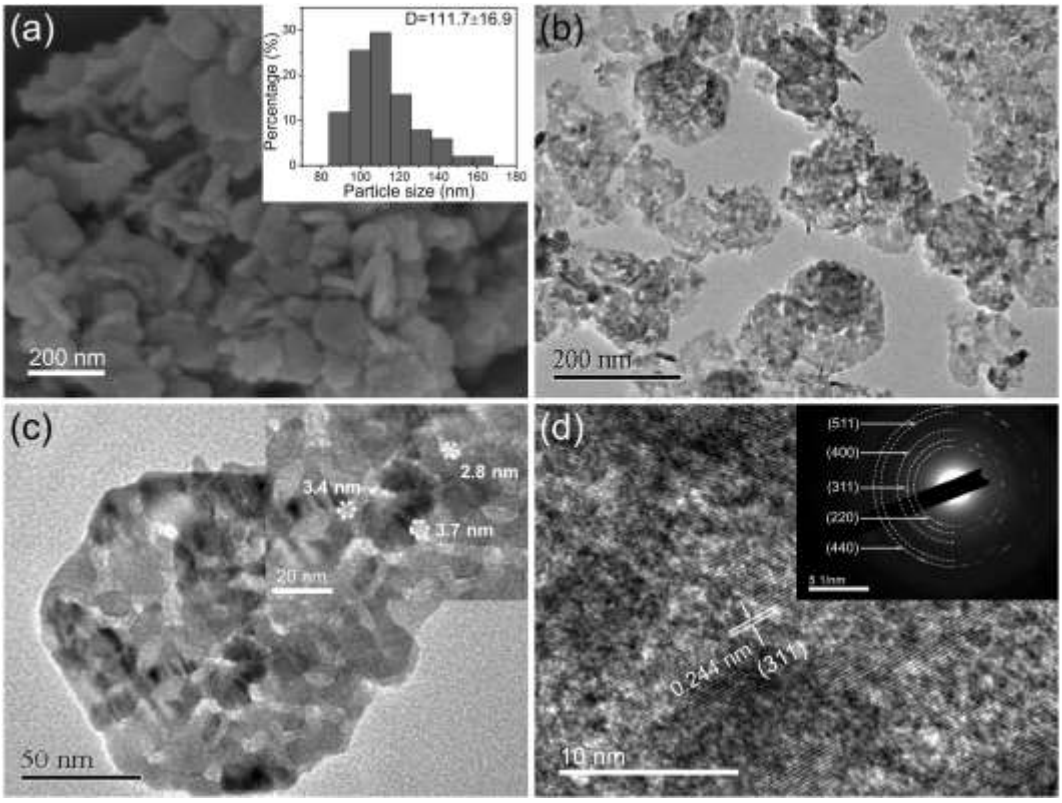

Fig. 1 SEM and TEM images of Co_3O_4 nanoplates. (a) SEM image, the inset shows the size distribution. (b-c) TEM images, the inset shows the pore size of the nanoplate (marked in white circles). (d) High-magnification TEM image with SAED (inset).

XRD has been conducted to further elucidate the crystalline structure of Co_3O_4 nanoplates. As shown in **Fig. 2a**, the peaks match those of spinel Co_3O_4 (JCPDS 42-1467), consistent with the results obtained from SAED. Due to the highly porous structure and small dimensions, the specific surface area of Co_3O_4 nanoplate researches a high value of 98.65 $m^2\ g^{-1}$ (**Fig. 2b**). The mesoporous structure was confirmed by the pore size distribution shown in **Fig. 2b** inset. The pore size of 2.6 nm is consistent with the TEM observation in **Fig. 1c**, and the pore volume is measured to be 0.628 $cm^3\ g^{-1}$. The high specific surface area associated with the mesoporous structure of the Co_3O_4 hexagonal nanoplates not only provides abundant reaction sites increases, but also increase the accessibility of the electrolyte to the active materials, which may help to enhance the electrochemical performance.

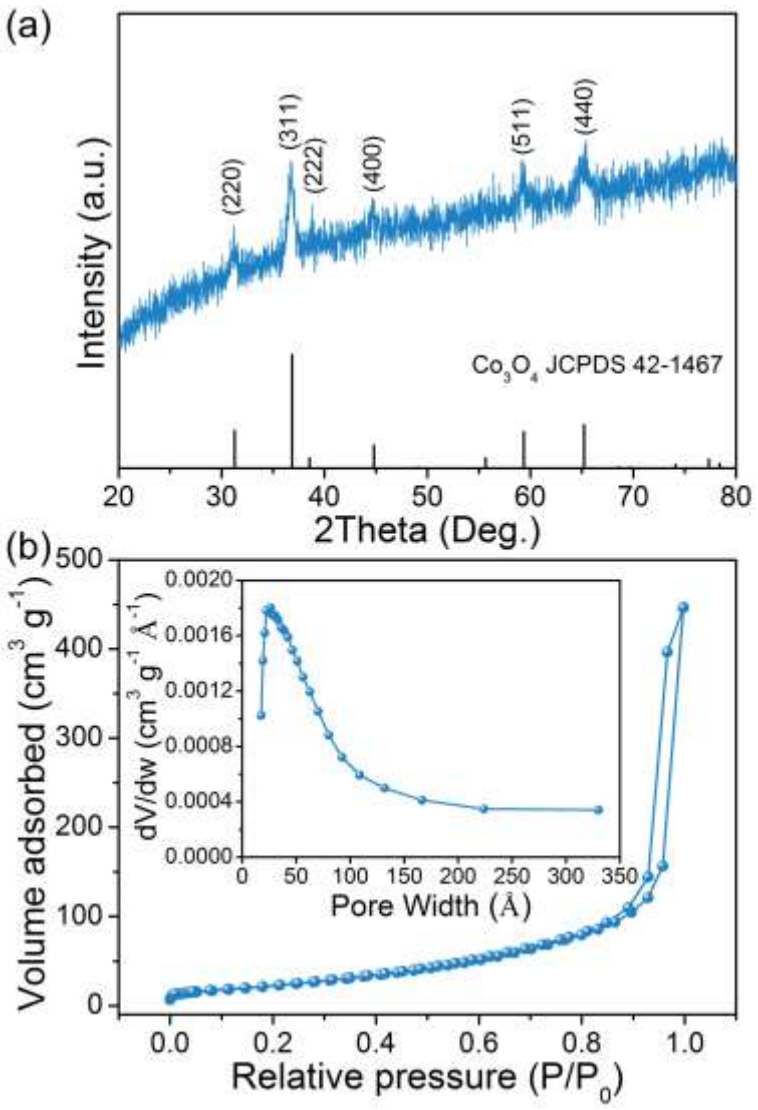

Fig. 2 Characterization of Co_3O_4 nanoplates. (a) XRD pattern. (b) Nitrogen adsorption-desorption isotherms, and the inset shows the pore size distribution.

3.2 Electrochemical properties

The ORR and OER activity of Co_3O_4 nanoplates was evaluated in 0.1 M KOH electrolyte, and compared with that of Pt/C. As shown in **Fig. 3a**, Co_3O_4 nanoplate exhibits a limiting current density of −5.18 mA cm^{-2} at 0.3 V (vs. RHE) in the ORR region, and the Tafel slope is 82.32 mV dec^{-1} (**Fig. 3a** inset). In comparison, the values achieved by the commercial Pt/C are −5.21 mA cm^{-2} and 66.90 mV dec^{-1}, respectively. Hence, the Co_3O_4 nanoplate presents the comparable ORR activity to that of Pt/C. **Fig.**

3b presents the LSV curves of the Co_3O_4 nanoplate at different rotating rates, and the inset presents the corresponding Koutecky-Levich plots. The average number of electrons transferred (n) is determined to be ~4, indicating a four-electron ORR process. In the OER region, the Co_3O_4 nanoplate possesses a Tafel slope of 77.9 mV dec^{-1} and achieves the current density of 10 mA cm^{-2} at 1.63 V (vs. RHE). Comparatively, the Tafel slope is 143.5 mV dec^{-1} for Pt/C, and the current density only reaches 4.5 mA cm^{-2} at a high potential of 1.77 V (vs. RHE). Hence, the potential to achieve 10 mA cm^{-2} of Co_3O_4 nanoplates is superior to those of some reported state-of-the-art catalysts (e.g., Fe@N-doped carbon nanoshell: 1.70 V [37]; Co and N co-doped carbon: 1.74 V [38]; FeCo@N-doped graphitic carbon nanotubes: 1.76 V [39]). The reversibility of the oxygen electrode can be evaluated by the potential gap (ΔE) between the half-wave potential in the ORR ($E_{1/2}$) and the potential at 10 mA cm^{-2} in the OER ($E_{j=10}$). Thus, the value of ΔE for Co_3O_4 nanoplates is calculated to be 0.84 V, which surpasses the noble metal-based catalysts (e.g., Ir/C: 1.41 V) [40] and some reported bifunctional catalysts [41–48], as listed in **Table S1**, demonstrating the high effectiveness as a bifunctional electrocatalyst.

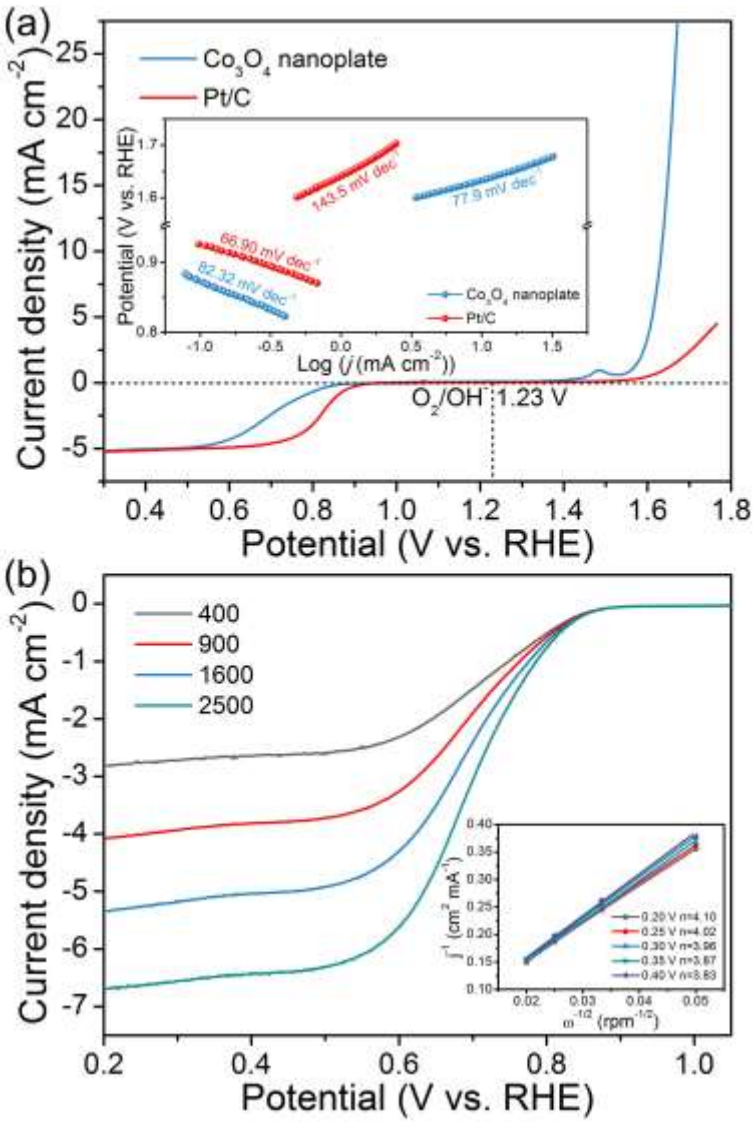

Fig. 3 Electrochemical activity of the Co_3O_4 nanoplate in 0.1 M KOH. (a) LSV curves in the O_2 saturated electrolyte, and the inset shows the corresponding Tafel plots. (b) RDE curves at different rotating rates, the inset shows the corresponding Koutecky-Levich plots.

It is worth noting that a small peak appears in the LSV curve of the OER region (**Fig. 3a**). To study the redox behavior of Co_3O_4 nanoplates, CV measurements were carried out within 0.3−0.8 V (vs. Hg/HgO) at various rates. As presented in **Fig. 4a**, the anodic and cathodic peaks in the non-rectangular shaped CV curves represent the oxidation and reduction processes, respectively. Previous works have indicated that Co_3O_4 can undergo the charge-transfer reactions of Co(II) ↔ Co(III) ↔ Co(IV) with

three redox couples of $Co_3O_4/Co(OH)_2$, Co_3O_4/CoOOH, and CoOOH/CoO_2 in alkaline solutions [49,50]. In the present study, only one couple of peaks instead of three is evident. This phenomenon is also reported in ref. [28] for the mesoporous layered hexagonal Co_3O_4 nanoparticles, which may be caused by the surface modification of Co_3O_4 [51] and/or the difference in alkaline concentration [49,50]. With an increase of the scan rate, the anodic and cathodic peaks gradually shift towards the positive and negative potential, respectively, and the current densities increase. The capacitance values at different scan rates are presented in **Fig. 4b**. At 5 mV s^{-1}, the capacitance is 330 F g^{-1}. Even at a high rate of 100 mV s^{-1}, the capacitance can still reach 275 F g^{-1}, from which the retention rate is calculated to be 83.3%. Comparatively, the hexagonal Co_3O_4 nanoparticles reported by Shirage *et al.* achieved the capacitance value of 305 and 180 mAh g^{-1} at 5 and 100 mV s^{-1}, respectively, with a retention rate of 59.0% [28]. Hence, the Co_3O_4 nanoplate in this work exhibited higher rate performance, which may come from the smaller particle size and larger surface area, shortening the lengths for ion and electron transport and increasing the active sites. To examine the redox stability, we also measured the CV curves at 50 mV s^{-1} for 2500 cycles. As illustrated in **Fig. 4c**, the peak current densities gradually decrease, while the shape of CV curves is well maintained. Through calculating the corresponding capacitance, it is found that the retention rate can still reach 60.3% even after 2500 cycles (**Fig. 4d**), showing a good stability [52]. The electrochemical properties demonstrated above, including excellent ORR and OER activity, a high pseudocapacitance, and a high capacitance retention rate, are crucial for the performance enhancement of Zn-air batteries [53].

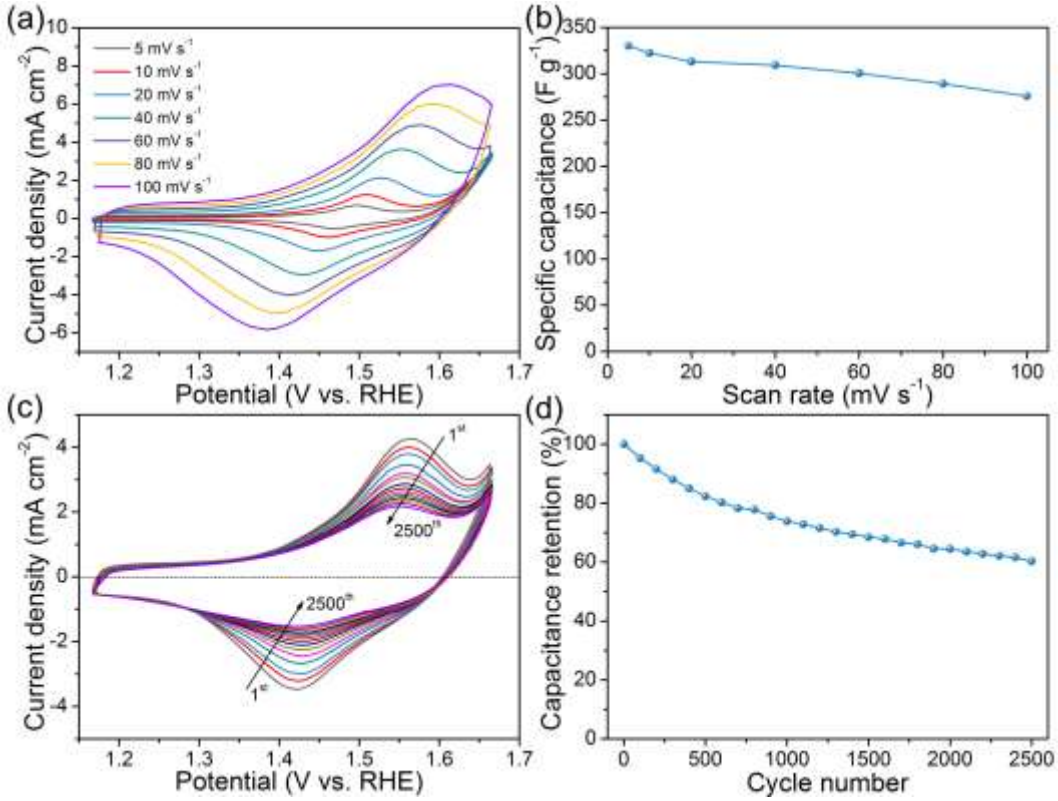

Fig. 4 CV measurements of the Co_3O_4 nanoplate electrode. (a) CV curves at various scan. (b) Variation of the specific capacitance. (c) Selected CV curves at the scan rate of 50 mV s^{-1}. (d) Capacitance retention rate during the cycle.

3.3 Battery performance

The performance of Co_3O_4 nanoplates and Pt/C as the catalyst materials was evaluated in a Zn-air battery. The polarization curves presented in **Fig. 5a** show that the maximum power density of Co_3O_4 nanoplate is 59.7 mW cm^{-2}, equal to 73.6% of that achieved by Pt/C (81.1 mW cm^{-2}). Using the current density of 1 mA cm^{-2}, both Co_3O_4 nanoplate and Pt/C result in good discharge voltage plateaus, and the final voltage drop is attributed to the consumption of the Zn metal. The Co_3O_4 nanoplate delivers a specific capacity of 702.4 mAh g_{Zn}^{-1} with a gravimetric energy density of 901.6 Wh kg_{Zn}^{-1} (**Fig. 5b**), which are higher than those obtained by Pt/C (640.0 mAh g_{Zn}^{-1}, 828.5 Wh kg_{Zn}^{-1}). For the charge process, as illustrated by the polarization curves in **Fig. 5a**, Co_3O_4 nanoplate delivers lower voltages than that of Pt/C. Even with a little higher loading (2

mg cm^{-2}) than that of the Co_3O_4 nanodisk electrode (ca. 1.5 mg cm^{-2}) reported by Chen *et al.* [26], the discharge voltage of the present Co_3O_4 nanoplate is improved and the charge voltage is remarkably reduced, indicating the high activity in the battery (**Fig. S3**). We further tested the discharge and charge performance of the Co_3O_4 nanoplate using 1 mA cm^{-2}. As shown in **Fig. 5c**, humps are observed in the voltage profiles, which are different from the conventional single plateau (e.g., Pt/C, **Fig. 5d**). The charge voltage exhibits a distinct plateau at 1.87 V, followed by a higher plateau at 1.96 V for the OER. While in the discharge process, a first voltage plateau exists at 1.80 V, followed by the plateau at 1.27 V for the ORR. This first higher voltage plateaus are consistent with the reported Zn-Co_3O_4 battery, which corresponds to the conversion between Co_3O_4 and CoO_2 [54]. Hence, the charge-discharge behaviors in Co_3O_4 nanoplate electrode originate from the oxidation-reduction of the cobalt oxide and the OER-ORR process, consistent with the electrochemical properties observed in **Fig. 4**, forming a hybrid Zn-M/air battery (M is the transition metal) as reported [53,55,56]. Due to the increased energy delivered on discharge and the decreased energy consumed on charge, the energy efficiency is calculated to be 67.3%, higher than that obtained by Pt/C (66.3%), even though Pt/C delivers the voltages of 1.95 and 1.30 V on the OER and ORR, respectively.

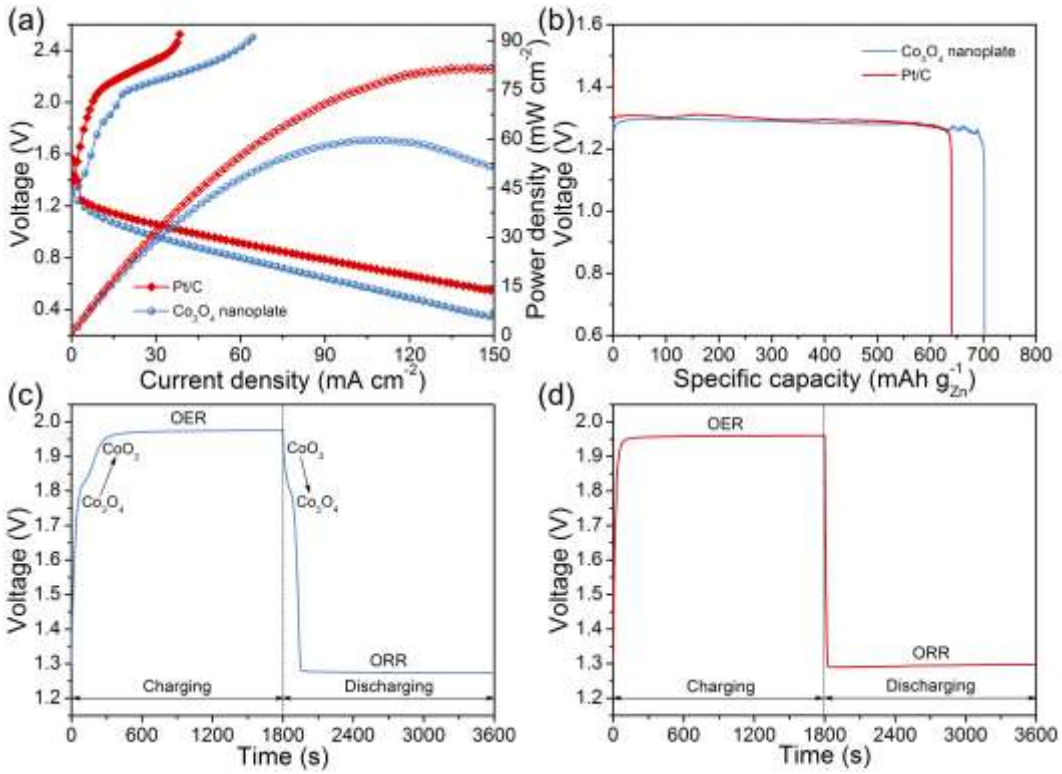

Fig. 5 Electrochemical characteristics of the Zn-air battery with Co_3O_4 nanoplates and Pt/C. (a) Polarization curves and power densities. (b) Discharge voltage curves at 1 mA cm^{-2}. (c-d) Charge-discharge voltage profiles at 1 mA cm^{-2} (30 min for charging and 30 min for discharging) of (c) Co_3O_4 nanoplates and (d) Pt/C.

The electrochemical durability of Co_3O_4 nanoplates in rechargeable Zn-air batteries was investigated by a pulse discharge-charge test at 10 mA cm^{-2}. As shown in **Fig. 6a**, a stable voltage profile is obtained for 100 cycles. On the contrary, the commercial Pt/C leads to a high charge voltage up to 2.3 V (**Fig. 6a**). Such a high voltage will cause the carbon corrosion and performance degradation, leading to the failure of the battery eventually. Consequently, starting from the 90th cycle, the discharge voltage quickly drops. For a clear comparison, as shown in **Fig. 6c**, the voltage gap of Co_3O_4 nanoplate at the 1st cycle is 0.917 V, and only increase to 0.946 V at the 100th cycle; while for Pt/C, the voltage gap enlarges from 1.074 V to 1.367 V. Even at the high current density, the metal oxide oxidation-reduction can still be observed (**Fig. 6c**), which benefits the discharge and charge processes. As a result, the energy efficiency of the battery with

Co_3O_4 nanoplates keeps stable at 58% during cycle (**Fig. 6d**), while it drops from 53% to 44% for Pt/C. These results emphasize the Co_3O_4 nanoplate as a highly efficient and stable active material for rechargeable Zn-air batteries.

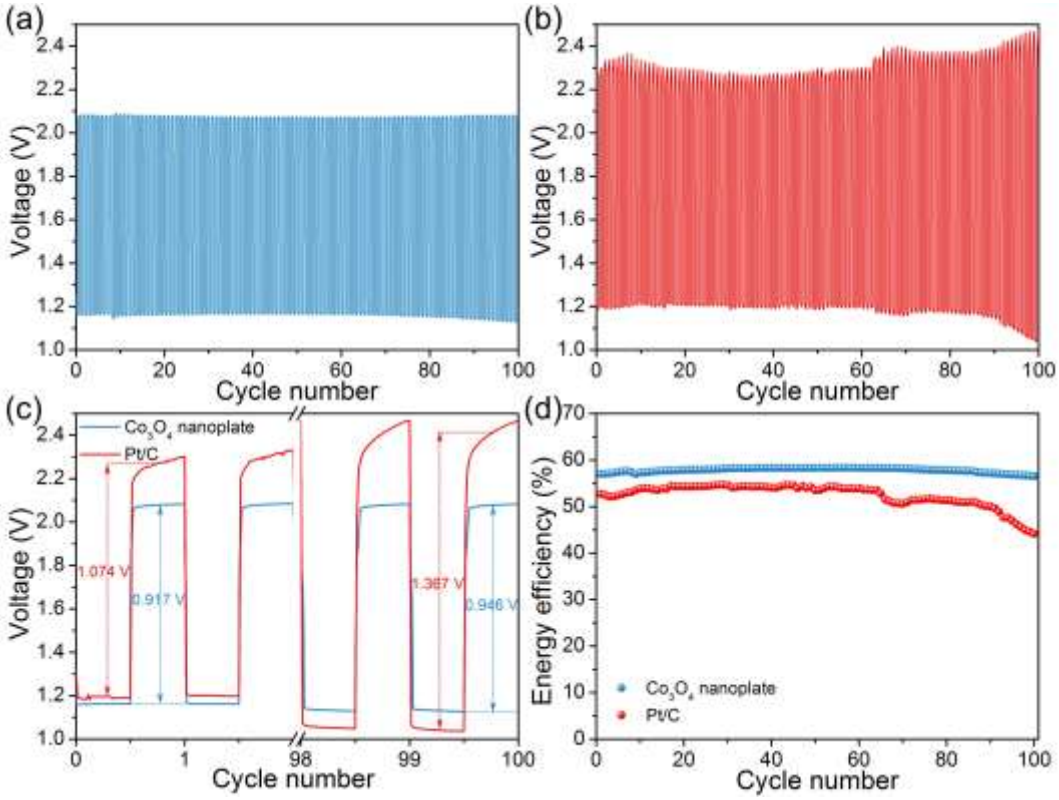

Fig. 6 Cycling stability of the Zn-air battery with Co_3O_4 nanoplates and Pt/C. (a-b) Cycling stability test at 10 mA cm^{-2} for 360 s discharge and 360 s charge: (a) Co_3O_4 nanoplates and (b) Pt/C. (c) Discharge-charge voltage profiles for the selected cycles. (d) Energy efficiency during the cycling test.

4. Conclusions

In summary, two-dimensional porous hexagonal Co_3O_4 nanoplates with the average size and thickness of ~100 and ~20 nm have been synthesized in this work. The large surface area and mesoporous nanostructures provide abundant active sites and shorten the lengths for ion and electron transport. In an alkaline solution, the Co_3O_4 nanoplate exhibited a limiting current density (−5.18 mA cm^{-2}) comparable to that of the commercial Pt/C (−5.21 mA cm^{-2}) in the ORR region and the superior activity with the

potential of 1.63 V at 10 mA cm^{-2} in the OER region. Additionally, redox reactions corresponding to the oxidation and reduction of cobalt species were observed, and the capacitance of 330 F g^{-1} and a high retention rate of 60.3% after 2500 cycles were delivered. A Zn-air battery with Co_3O_4 nanoplates as the active material delivered the maximum power density of 59.7 mW cm^{-2} and the gravimetric energy density of 901.6 Wh kg_{Zn}^{-1}. Through synergizing the activity towards the oxygen electrocatalysis and the supercapacitive behavior, the oxidation-reduction of cobalt oxides and the OER-ORR process were exhibited during charge and discharge, resulting in the higher energy efficiency (67.3%) than that of commercial Pt/C (66.3%). Moreover, the low voltage gaps between discharge and charge as well as the high energy efficiency of 58% at 10 mA cm^{-2} were maintained for 100 cycles. The results demonstrate that the porous Co_3O_4 nanoplate is a potential active material for efficient rechargeable Zn-air batteries with excellent cycling stability and high energy density.

Acknowledgments

P. Tan thanks the funding support from CAS Pioneer Hundred Talents Program. M. Ni thanks the funding support from The Hong Kong Polytechnic University (G-YBJN and G-YW2D), a fund from RISUD (1-ZVEA), and a grant (Project Number: PolyU 152214/17E) from Research Grant Council, University Grants Committee, Hong Kong SAR.

References

[1] Dunn B, Kamath H, Tarascon J-M. Electrical Energy Storage for the Grid: A Battery of Choices. Science 2011;334:928–35.

[2] Tan P, Chen B, Xu H, Zhang H, Cai W, Ni M, et al. Flexible Zn– and Li–air

batteries: recent advances, challenges, and future perspectives. Energy Environ Sci 2017;10:2056–80.

[3] Ye L, Lv W, Zhang KHL, Wang X, Yan P, Dickerson JH, et al. A new insight into the oxygen diffusion in porous cathodes of lithium-air batteries. Energy 2015;83:669–73.

[4] Kondoh J, Ishii I, Yamaguchi H, Murata A, Otani K, Sakuta K, et al. Electrical energy storage systems for energy networks. Energy Convers Manag 2000;41:1863–74.

[5] Liu Z, Li Z, Ma J, Dong X, Ku W, Wang M, et al. Nitrogen and cobalt-doped porous biocarbon materials derived from corn stover as efficient electrocatalysts for aluminum-air batteries. Energy 2018;162:453–9.

[6] Xu H, Chen B, Tan P, Zhang H, Yuan J, Liu J, et al. Performance improvement of a direct carbon solid oxide fuel cell system by combining with a Stirling cycle. Energy 2017;140:979–87.

[7] Liu B, Xu W, Yan P, Kim ST, Engelhard MH, Sun X, et al. Stabilization of Li Metal Anode in DMSO-Based Electrolytes via Optimization of Salt-Solvent Coordination for Li-O_2 Batteries. Adv Energy Mater 2017:1602605.

[8] Li Y, Dai H. Recent advances in zinc–air batteries. Chem Soc Rev 2014;43:5257–75.

[9] Tan P, Wei Z, Shyy W, Zhao TS. Prediction of the theoretical capacity of non-aqueous lithium-air batteries. Appl Energy 2013;109:275–82.

[10] Fu J, Cano ZP, Park MG, Yu A, Fowler M, Chen Z. Electrically Rechargeable Zinc-Air Batteries: Progress, Challenges, and Perspectives. Adv Mater

2017;29:1604685.

[11] Lee J-S, Kim ST, Cao R, Choi N-S, Liu M, Lee KT, et al. Metal-Air Batteries with High Energy Density: Li-Air versus Zn-Air. Adv Energy Mater 2011;1:34–50.

[12] Jung CY, Kim TH, Kim WJ, Yi SC. Computational analysis of the zinc utilization in the primary zinc-air batteries. Energy 2016;102:694–704.

[13] Tan P, Jiang HR, Zhu XB, An L, Jung CY, Wu MC, et al. Advances and challenges in lithium-air batteries. Appl Energy 2017;204:780–806.

[14] Cheng F, Chen J. Metal–air batteries: from oxygen reduction electrochemistry to cathode catalysts. Chem Soc Rev 2012;41:2172–92.

[15] Miao H, Wang Z, Wang Q, Sun S, Xue Y, Wang F, et al. A new family of Mn-based perovskite ($La_{1-x}Y_xMnO_3$) with improved oxygen electrocatalytic activity for metal-air batteries. Energy 2018;154:561–70.

[16] Ma Z, Wang K, Qiu Y, Liu X, Cao C, Feng Y, et al. Nitrogen and sulfur co-doped porous carbon derived from bio-waste as a promising electrocatalyst for zinc-air battery. Energy 2018;143:43–55.

[17] Li J-C, Wu X-T, Chen L-J, Li N, Liu Z-Q. Bifunctional MOF-derived Co-N-doped carbon electrocatalysts for high-performance zinc-air batteries and MFCs. Energy 2018;156:95–102.

[18] Du G, Liu X, Zong Y, Hor TSA, Yu A, Liu Z. Co_3O_4 nanoparticle-modified MnO_2 nanotube bifunctional oxygen cathode catalysts for rechargeable zinc–air batteries. Nanoscale 2013;5:4657–61.

[19] Wang Y, Ma X, Lu L, He Y, Qi X, Deng Y. Carbon supported MnO_x-Co_3O_4 as cathode catalyst for oxygen reduction reaction in alkaline media. Int J Hydrogen

Energy 2013;38:13611–6.

[20] Mainar AR, Colmenares LC, Leonet O, Alcaide F, Iruin JJ, Weinberger S, et al. Manganese oxide catalysts for secondary zinc air batteries: from electrocatalytic activity to bifunctional air electrode performance. Electrochim Acta 2016;217:80–91.

[21] Wu MC, Zhao TS, Jiang HR, Wei L, Zhang ZH. Facile preparation of high-performance MnO_2/KB air cathode for Zn-air batteries. Electrochim Acta 2016;222:1438–44.

[22] Wang Q, Shang L, Shi R, Zhang X, Zhao Y, Waterhouse GIN, et al. NiFe Layered Double Hydroxide Nanoparticles on Co,N-Codoped Carbon Nanoframes as Efficient Bifunctional Catalysts for Rechargeable Zinc-Air Batteries. Adv Energy Mater 2017;7:1700467.

[23] Singh SK, Dhavale VM, Kurungot S. Surface-Tuned Co_3O_4 Nanoparticles Dispersed on Nitrogen-Doped Graphene as an Efficient Cathode Electrocatalyst for Mechanical Rechargeable Zinc–Air Battery Application. ACS Appl Mater Interfaces 2015;7:21138–49.

[24] Li B, Ge X, Goh FWT, Hor TSA, Geng D, Du G, et al. Co_3O_4 nanoparticles decorated carbon nanofiber mat as binder-free air-cathode for high performance rechargeable zinc-air batteries. Nanoscale 2015;7:1830–8.

[25] He Y, Zhang J, He G, Han X, Zheng X, Zhong C, et al. Ultrathin Co_3O_4 nanofilm as an efficient bifunctional catalyst for oxygen evolution and reduction reaction in rechargeable zinc–air batteries. Nanoscale 2017;9:8623–30.

[26] Su D, Dou S, Wang G. Single Crystalline Co_3O_4 Nanocrystals Exposed with

Different Crystal Planes for Li-O_2 Batteries. Sci Rep 2015;4:5767.

[27] Lee DU, Scott J, Park HW, Abureden S, Choi JY, Chen Z. Morphologically controlled Co_3O_4 nanodisks as practical bi-functional catalyst for rechargeable zinc-air battery applications. Electrochem Commun 2014;43:109–12.

[28] Bhojane P, Sinha L, Devan RS, Shirage PM. Mesoporous layered hexagonal platelets of Co_3O_4 nanoparticles with (111) facets for battery applications: high performance and ultra-high rate capability. Nanoscale 2018;10:1779–87.

[29] Zhou X, Xia Z, Tian Z, Ma Y, Qu Y. Ultrathin porous Co_3O_4 nanoplates as highly efficient oxygen evolution catalysts. J Mater Chem A 2015;3:8107–14. doi:10.1039/C4TA07214F.

[30] Gou W, Zhou X, Li J, Ma Y. Nanoporous Co_3O_4 plates as highly electroactive materials for electrochemical energy storage. Mater Lett 2016;180:207–11.

[31] Zeng L, Zhao TS, An L. A high-performance supportless silver nanowire catalyst for anion exchange membrane fuel cells. J Mater Chem A 2015;3:1410–6.

[32] Salunkhe RR, Lin J, Malgras V, Dou SX, Kim JH, Yamauchi Y. Large-scale synthesis of coaxial carbon nanotube/$Ni(OH)_2$ composites for asymmetric supercapacitor application. Nano Energy 2015;11:211–8.

[33] Meng F, Zhong H, Bao D, Yan J, Zhang X. In Situ Coupling of Strung Co_4N and Intertwined N–C Fibers toward Free-Standing Bifunctional Cathode for Robust, Efficient, and Flexible Zn–Air Batteries. J Am Chem Soc 2016;138:10226–31.

[34] Tan P, Shyy W, Wei ZH, An L, Zhao TS. A carbon powder-nanotube composite cathode for non-aqueous lithium-air batteries. Electrochim Acta 2014;147:1–8.

[35] Tan P, Chen B, Xu H, Cai W, He W, Liu M, et al. Co_3O_4 Nanosheets as Active

Material for Hybrid Zn Batteries. Small 2018;14:1800225.

[36] Zhu Z, Ping J, Huang X, Hu J, Chen Q, Ji X, et al. Hexagonal nickel oxide nanoplate-based electrochemical supercapacitor. J Mater Sci 2012;47:503–7.

[37] Wang J, Wu H, Gao D, Miao S, Wang G, Bao X. High-density iron nanoparticles encapsulated within nitrogen-doped carbon nanoshell as efficient oxygen electrocatalyst for zinc–air battery. Nano Energy 2015;13:387–96.

[38] Hu W, Wang Q, Wu S, Huang Y. Facile one-pot synthesis of a nitrogen-doped mesoporous carbon architecture with cobalt oxides encapsulated in graphitic layers as a robust bicatalyst for oxygen reduction and evolution reactions. J Mater Chem A 2016;4:16920–7.

[39] Su C-Y, Cheng H, Li W, Liu Z-Q, Li N, Hou Z, et al. Atomic Modulation of FeCo-Nitrogen-Carbon Bifunctional Oxygen Electrodes for Rechargeable and Flexible All-Solid-State Zinc-Air Battery. Adv Energy Mater 2017;7:1602420.

[40] Aijaz A, Masa J, Rösler C, Xia W, Weide P, Botz AJR, et al. Co@Co_3O_4 Encapsulated in Carbon Nanotube-Grafted Nitrogen-Doped Carbon Polyhedra as an Advanced Bifunctional Oxygen Electrode. Angew Chemie Int Ed 2016;55:4087–91.

[41] Wang Q, Lei Y, Chen Z, Wu N, Wang Y, Wang B, et al. Fe/Fe_3C@C nanoparticles encapsulated in N-doped graphene–CNTs framework as an efficient bifunctional oxygen electrocatalyst for robust rechargeable Zn–air batteries. J Mater Chem A 2018;6:516–26.

[42] Masa J, Xia W, Sinev I, Zhao A, Sun Z, Grützke S, et al. Mn_xO_y/NC and Co_xO_y/NC Nanoparticles Embedded in a Nitrogen-Doped Carbon Matrix for High-

Performance Bifunctional Oxygen Electrodes. Angew Chemie Int Ed 2014;53:8508–12.

[43] Deng YP, Jiang Y, Luo D, Fu J, Liang R, Cheng S, et al. Hierarchical Porous Double-Shelled Electrocatalyst with Tailored Lattice Alkalinity toward Bifunctional Oxygen Reactions for Metal-Air Batteries. ACS Energy Lett 2017;2:2706–12.

[44] Tang C, Wang H-F, Chen X, Li B-Q, Hou T-Z, Zhang B, et al. Topological Defects in Metal-Free Nanocarbon for Oxygen Electrocatalysis. Adv Mater 2016;28:6845–51.

[45] Seo B, Sa YJ, Woo J, Kwon K, Park J, Shin TJ, et al. Size-Dependent Activity Trends Combined with in Situ X-ray Absorption Spectroscopy Reveal Insights into Cobalt Oxide/Carbon Nanotube-Catalyzed Bifunctional Oxygen Electrocatalysis. ACS Catal 2016;6:4347–55.

[46] Liu Q, Jin J, Zhang J. $NiCo_2S_4$@graphene as a Bifunctional Electrocatalyst for Oxygen Reduction and Evolution Reactions. ACS Appl Mater Interfaces 2013;5:5002–8

[47] Zhang J, Zhao Z, Xia Z, Dai L. A metal-free bifunctional electrocatalyst for oxygen reduction and oxygen evolution reactions. Nat Nanotechnol 2015;10:444.

[48] Han S, Hu X, Wang J, Fang X, Zhu Y. Novel Route to Fe-Based Cathode as an Efficient Bifunctional Catalysts for Rechargeable Zn-Air Battery. Adv Energy Mater 2018;8:1800955.

[49] Casella IG, Gatta M. Study of the electrochemical deposition and properties of cobalt oxide species in citrate alkaline solutions. J Electroanal Chem 2002;534:31–

8.

[50] Nkeng P. Characterization of Spinel-Type Cobalt and Nickel Oxide Thin Films by X-Ray Near Grazing Diffraction, Transmission and Reflectance Spectroscopies, and Cyclic Voltammetry. J Electrochem Soc 1995;142:1777–83.

[51] Castro EB, Gervasi CA, Vilche JR. Oxygen evolution on electrodeposited cobalt oxides. J Appl Electrochem 1998;28:835–41.

[52] Wu YP, Wang X, Li M, Wang Y, Chen B, Zhu Y. A Zn-NiO rechargeable battery with long lifespan and high energy density. J Mater Chem A 2015;3:8280–3.

[53] Qaseem A, Chen F, Qiu C, Mahmoudi A, Wu X, Wang X, et al. Reduced Graphene Oxide decorated with Manganese Cobalt Oxide as Multifunctional Material for Mechanically Rechargeable and Hybrid Zinc-Air Batteries. Part Part Syst Charact 2017;34:1700097.

[54] Wang X, Wang F, Wang L, Li M, Wang Y, Chen B, et al. An Aqueous Rechargeable Zn//Co_3O_4 Battery with High Energy Density and Good Cycling Behavior. Adv Mater 2016;28:4904–11.

[55] Lee DU, Fu J, Park MG, Liu H, Ghorbani Kashkooli A, Chen Z. Self-Assembled NiO/$Ni(OH)_2$ Nanoflakes as Active Material for High-Power and High-Energy Hybrid Rechargeable Battery. Nano Lett 2016;16:1794–802.

[56] Li B, Quan J, Loh A, Chai J, Chen Y, Tan C, et al. A robust hybrid zn-battery with ultralong cycle life. Nano Lett 2017;17:156–63.